Assessment of Induced Voltages in Common and Differential-Mode for a PV Module due to Nearby Lightning Strikes

A. Formisano [1], C. Petrarca[2], J.C. Hernández[3*], F.J. Muñoz-Rodríguez[4]

[1] Dept. of Engineering, Univ. della Campania "Luigi Vanvitelli", via Roma 29, Aversa 81031, Italy
[2] Dept. of Electrical and Information Technology Engineering, Univ. di Napoli "Federico II", via Claudio 21, Napoli 80125, Italy
[3] Dept. of Electrical Engineering, University of Jaen, Campus Lagunillas s/n, Edificio A3, Jaén 23071, Spain
[4] Dept, of Electronic and Automatic Engineering, University of Jaen, Campus Lagunillas s/n, Edificio A3, Jaén 23071, Spain
[*] jcasa@ujaen.es

Abstract: Nearby lightning strikes are prone to induce overvoltage transients in Photovoltaic (PV) modules and in their power conditioning circuitry, which can permanently damage the PV system. Therefore, it becomes important to establish a method for accurate assessment of such transients. To this aim, we propose a three-dimensional (3D) semi-analytical numerical method to study the electromagnetic transients caused in PV modules by nearby lightning strikes. The approach bases on a semi-analytical expression of the magnetic vector potential generated by a geometrically complex lightning channel. The proposed method is able to calculate the transient overvoltage in a PV module, both in common and differential-mode, taking also into account capacitive and inductive couplings between the internal circuit and the PV metallic frame. Both modes are required to design the surge protective devices (SPDs) in PV power systems. Comparing to the models in literature, the proposed approach explicitly considers the complex geometry of the lightning channel. Statistical analysis allows assessing the impact of channel geometry by randomly generating a number of likely lightning paths. Results show that the lightning induced overvoltage in a PV module is highly dependent on factors such as distance to the lightning channel and lightning channel geometry.

Keywords: Photovoltaic power system, lightning protection, transient response, electromagnetic fields, computer aided analysis.

1. Introduction

PV power systems are typically located on either roofs or facades of buildings or as freestanding installations. Therefore, direct or nearby lightning strikes are prone to hit them during thunderstorms [1,2]. The events of strikes hitting nearby the PV system, more frequent than direct strikes, proved to cause non-negligible damages to the PV circuitry and structures [3]. These phenomena still need accurate analysis for an effective design of the lightning and surge protection.

As a matter of fact, PV power systems have many conducting wires and massive metallic parts: DC cables, internal circuitry, modules metal frame, metallic support construction, grounding systems, lightning protection system (LPS) and so on. The conductors couple with electromagnetic fields associated with Lightning ElectroMagnetic Pulse (LEMP), which can release significant amounts of electromagnetic energy to the PV module yet without direct current flow [2,4-6]. This may result in the dielectric breakdown of PV modules [2,7,8] or in power conditioner and measurement circuity malfunctioning [9-11]. Surge withstand capability (SWC) [2,12-15] quantifies the overvoltage level induced by direct or nearby lightning strikes that the PV dielectric materials [16, 17] can withstand without damage. Numerical simulations can help understand under which circumstances the induced voltages exceed the SWC, helping to establish appropriate lightning and surge protection schemes [2, 18-21].

Computational analysis of electromagnetic fields is applied to model their interaction fields with the objects and the environment using Maxwell's equations. Numerical methods for analysing lightning-caused electromagnetic transients in conducting structures can be broadly classified according to two methodologies [22]: transmission-line models [23,24] and full-wave models. The former one assumes transverse electromagnetic waves (TEM mode), and easily interfaces with a circuit simulator, but requires lumped models to treat coupling among conductors. In contrast, the latter one is capable of modelling all the electromagnetic coupling mechanisms in soil or air at the price of much more complicated numerical models.

Full-wave models [25] include integral equation methods solved by method of Moments (MoM) [26] and Modified-Mesh-Current method (MMC) [27, 28], differential equation methods can be solved by Finite Element Method (FEM) [29,30], Finite-Difference Time-Domain (FDTD) method [31, 32], Boundary Element Method (BEM) [33]. Conversely, under suited simplifying assumptions detailed in Section 2, analytical solutions providing fields from simple sources (e.g. Hertzian dipoles) can be used to establish semi-analytical methods, capable of overcoming many of the drawbacks of fully numerical methods. Combinations of MoM [34], MMC [35] and FDTD [36-38] together with analytical approaches [39] have been widely used in calculating lightning-induced transient overvoltage on power system (e.g. in LPS and/or on overhead lines).

On the other hand, there are a few studies about overvoltage occurring when lightning directly hits PV power systems (either PV modules, support structure or LPS) based on MMC [40,41] and FDTD methods [42,43] or analytical methods [44- 48].

These works focus on the assessment of lightning induced voltages in the loops formed by internal circuit of PV modules in the PV array. They evaluate the impact of different aspects of the event, such as:

(i) the design of LPS and grounding system [40,41];
(ii) the lightning strike point [40,42,44-46];
(iii) the lightning current distribution in the metallic support mesh [41,44];
(iv) the lightning current amplitude and waveform [40,44];
(v) the soil resistivity [40,42,43];
(vi) the height above the ground [43].

Complementary, other works [49-5052] focus on the experimental assessment of just one among the above cited aspects.

A review of the PV literature [40-52] allows to disclose that just some references [43,44,53] assessed the overvoltage induced by nearby lightning strikes. Note that research in [43] did perform the study using a vertical straight segment to model the lightning channel (LC). In contrast, studies about direct strikes on PV power systems, assume a geometry determined by the LPS or the support structure, made by grounded metallic beams. To our best knowledge, no paper has yet specifically assessed the effects of tortuosity [54] of lightning discharges.

As concerning the metallic parts inside PV module, to analyse EM couplings of PV modules, the most adopted model treats the PV module as a single conducting loop [40-53], allowing differential-mode computation only [2]. The simplified model does not consider the inner structure of PV modules, their metal frames, and other elements. Focusing on the modelling of single PV modules for transient studies, most studies in literature [16] used simplified models with an internal conductor loop as well. Reference [17] only accounts a capacitive coupling.

In our opinion, such a simplified approach may lead to inaccurate results due to the inductive coupling between the internal PV module circuitry (the standard loop described above) and its metallic frame, which provides some shielding, especially against magnetic flux coupling.

Furthermore, to our best knowledge, capacitive coupling among metallic parts inside and around the PV module [41,55-57] is never considered. This implies a lack of knowledge about voltages between metallic frame and inner conducting loop (common-mode voltages), in spite of its relevance for the SPD choice in PV systems [2].

In this context, this research proposes a three-dimensional (3D) semi-analytical method to study the electromagnetic transients caused by lightning strikes hitting nearby to a PV module, based on the decomposition of the LC into a number of Hertzian dipoles. The proposed method is able to calculate the LC-induced transient overvoltage in a PV module, in common and differential-mode, considering both capacitive and inductive couplings between the internal circuit of PV module and its metallic frame. The PV module is modelled with thin-wire structures achieving good representational capacity of previous-mentioned elements. Comparing to the models in literature, results of proposed method are more accurate and cover broader voltage modes, which are required when choosing the surge protective devices (SPDs) for PV power systems [2]. Additionally, the impact of complex geometry of the LC is assessed through statistical analysis under a Monte Carlo approach by randomly generating a number of likely lightning path geometries.

The analysis is limited to the return stroke phase since the main damages to electrical/electronic systems (type of damage D_3 [58]) and, obviously, to its occupants (damage D_1 [58]) are due to the extremely high currents generated during this phase. Just the LC is considered, which amounts to considering the case of an unprotected PV system or the case of a strike hitting one of the poles close enough to be relevant.

The PV module is supposed to lay above the ground, tilted by a fixed angle to take best advantage of local solar irradiation. In addition, just the inductive coupling with the strike is considered for the overvoltage computation, while electric field map is computed inside the PV structure using a 3D FEM model to assess capacitive effects. This is justified by the "vertical" dimension of the PV module, not able to generate relevant voltage across PV module, although in the presence of high amplitude electric fields [59].

The paper is organized as follows: Section 2 describes the geometric model used to generate the LC, and the mathematical model used to compute magnetic field; Section 3 presents the geometrical model of the PV module and its internal electrical wiring scheme; Section 4 discusses the coupling between LC and PV module; Section 5 is dedicated to the method validation while in Section 6 an example of the capabilities of the proposed approach, including a statistical analysis of induced voltages, is illustrated and commented.

2. Modelling of magnetic field produced by a lightning channel

The coupling phenomena between the LC and the PV module, due to the difference of energies in the strike current and in the current flowing in the PV module circuitry, can be reasonably considered one-directional, the lightning strike inducing a largely more relevant voltage on PV than the other way around. We assume here that the highest spectral component in the lightning current is low enough (tens of MHz) to model the area enclosed by the PV module as electrically small, and no magnetic materials are present. Under these hypotheses, the induced voltage can be computed by time derivation of the line integral of the vector potential generated by the LC along the conducting segments composing the PV module circuitry (and possibly the metallic frame) [60] In this section the relevant aspects of models for the computation of the induced voltage are provided.

2.1. Geometrical model of the lightning-channel

Lightning is a transient, high-current electric discharge whose path length can reach some kilometres, air acting as an insulator between the positive and negative charges induced on the clouds and on the ground respectively. When the electric field distribution generated by the opposite charges reaches a critical value, the insulating capacity of the air breaks down, generating the

lightning discharge. Many studies have investigated on the effect of the LEMP due to the characteristics of the lightning channel, such as its inclination [61,62] and, more recently, its tortuosity [63,64,65]. LC tortuosity can significantly affect the generated fields and consequently the induced voltages. At close distance, their amplitude and frequency content mainly depend on the number and inclination of the LC bottom segments and on the relative position of the observer [54]. At larger distances [66], the sections of the LC farther from the ground become relevant, and propagation delays start to shape the induced voltages in a complex way, depending on size and orientation of different channel segments.

In the approach proposed here, the LC is represented as a segmented line starting from the clouds, acting as a charge reservoir, and touching earth near a PV array. The geometric model of the LC is generated by randomly defining number and position along the channel of a set of breaking points (see Fig. 1a for an example; dimensions of LC and PV module are not in scale).

During the generation of the geometric model, at each break point P_b three random numbers are generated, from a Gaussian distribution, namely the length L_s of the segment and the angles β_1 and β_2 with respect to the previous direction (see, Fig. 1b). Average of angles is zero, while average of length is given by $\lambda_{min}/10$, where λ_{min} is the smallest wavelength involved in the lighting current waveform. Standard deviations $(\sigma_{\beta_1}, (\sigma_{\beta_2}, \sigma_{\lambda min})$ act as "shaping" parameters for the LC [67]. The ground is assumed as a perfect conductor, and modelled using the images method, thus generating an additional set of "mirror" segments.

It is worth noting that the lightning can also hit the protection system. In this case, the additional path constituted by the pole of the protection system can be simulated by using additional straight segments; this latter aspect is not considered in the present paper since the focus point is on the modelling of the random part of the channel; it will be the subject of future work.

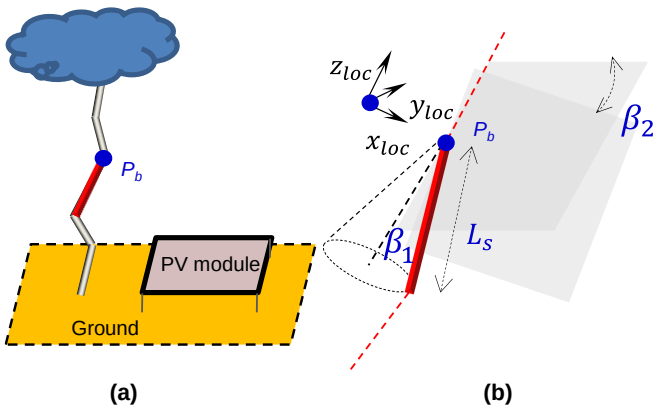

Fig. 1. ***(a)*** *Geometry of the LC and of PV module,* ***(b)*** *Definition of random parameters in LC creation*

2.2. *Electromagnetic modelling of the of the lightning-channel*

In the present work, we adopt the semi-analytical approach described in [68] (for EM fields calculation). The approach requires an analytical expression for the time and space dependence of the discharge current travelling along each vertical LC segment ***C***, of length h (Fig. 2a). In the assumed hypothesis of linear media, the (retarded) vector potential at point ***P*** due to a LC segment can be computed by using the (Lorentz gauged) expression of the vector potential ***A*** from a Hertzian dipole [69] and summing up all segment contributions.

A simple expression for the Hertzian dipole vector potential can be achieved if we assume a vertical LC segment of height h travelled by a step current of amplitude I_0 and velocity $v(t)$ (Fig. 2a):

$$i(z',t) = I_0 \left[u\left(t - \frac{z'}{v}\right)\right] [u(z') - u(z'-h)] \qquad (1)$$

where z' is the local z coordinate on the LC segment and $u(t)$ is the Heaviside step function. The current propagation velocity v along the channel is here assumed equal to one third of the light speed in vacuum c = 2.98 x10^9 m/s.

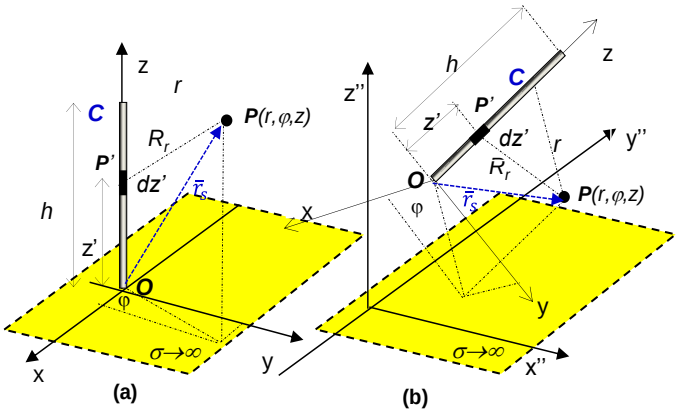

Fig. 2. ***(a)*** *Vertical discharge channel segment,* ***(b)*** *Arbitrarily oriented discharge channel segment*

In this simple case the vector potential $\boldsymbol{A}(\bar{r}_s, t)$ is directed along the z-axis and is φ independent:

$$\boldsymbol{A}(\bar{r}_s, t) = \frac{\mu_0}{4\pi} \int_0^h \frac{I_0 u\left(t - \frac{R_r}{c} - \frac{z'}{v}\right)}{R_r} dz' \, \hat{\boldsymbol{i}}_z \qquad (2)$$

where $R_r = \sqrt{(x-x')^2 + (y-y')^2 + (z-z')^2}$ is the distance between the source point ***P'***=(x',y',z') on the segment and the field point ***P***=(x,y,z) in the local cylindrical frame, $\hat{\boldsymbol{i}}_z$ is the unit vector associated to the direction of the segment, and μ_0 is the vacuum permeability.

The value of $\boldsymbol{A}(\bar{r}_s, t)$ depends on the integrand:

$$u\left(t - \frac{R_r}{c} - \frac{z'}{v}\right) = \begin{cases} 0 & if \left(t - \frac{R_r}{c} - \frac{z'}{v}\right) < 0 \\ 1 & if \left(t - \frac{R_r}{c} - \frac{z'}{v}\right) \geq 0 \end{cases} \qquad (3)$$

in which the function $\left(t - \frac{R_r}{c} - \frac{z'}{v}\right)$ is strictly decreasing with a zero value at:

$$z_0(t) = \frac{\frac{t}{v} - \frac{z}{c^2} - \sqrt{\left(\frac{t}{v} - \frac{z}{c^2}\right)^2 - \left(\frac{1}{v^2} - \frac{1}{c^2}\right)\left(t^2 - \frac{r^2}{c^2} - \frac{z^2}{c^2}\right)}}{\left(\frac{1}{v^2} - \frac{1}{c^2}\right)} \qquad (4)$$

Following the above consideration, we get:

$$\boldsymbol{A}(\bar{r}_s, t) = \begin{cases} 0 & if\ z' > z_0 \\ \frac{\mu_0}{4\pi} I_0 \int_0^{\min(h, z_0)} \frac{1}{R_r} dz' \hat{\boldsymbol{i}}_z & if\ z' \leq z_0 \end{cases} \qquad (5)$$

The calculation of (5), in the case in which $z' \leq 0$, is easy if we assume $\alpha = \text{atan}\left(\frac{z'-z}{r}\right)$:

$$\frac{\mu_0}{4\pi}\int_0^{\min(h,z_0)} \frac{I_0}{R_r} dz' = \frac{\mu_0 I_0}{4\pi}\int_{\alpha_1}^{\alpha_2} \frac{d\alpha}{\cos\alpha} = \left[\ln\sqrt{\frac{(1+\sin\alpha)}{(1-\sin\alpha)}}\right]_{\alpha_1}^{\alpha_2} \quad (6)$$

in which $\alpha_1 = \text{atan}(-\frac{z}{r})$ and $\alpha_2 = \text{atan}[\left(\frac{\min(h,z_0)-z}{r}\right)]$

The segment is then "mirrored" to take into account the perfectly conducting ground, and the final value of the vector potential generated by the channels computed by summing up the "direct" and the "mirrored" contributions [70].

This simple analytical formula for the vector potential can also be used for each segment composing a tortuous LC. In fact, each segment can be treated separately and the calculations are made by using a proper cylindrical coordinate system (Fig. 2b) originating from the starting point ***O*** of the channel segment, and whose *z*-axis is coincident with its axis. A suitable coordinate transformation is so required at each segment to combine different contributions in all space.

The vector potential is then calculated by adding the contributions of each segment and of its corresponding "image". Moreover, the calculation of the potential due to a generic current $i(t)$ propagating along the channel can be performed by the Duhamel's theorem and convolution summation [71]. The adopted current waveform is given in Section 2.3.

2.3. Lightning current waveform

The LC is modelled according to the Transmission line (TL) [72] hypothesis, that is the current propagates upward from the hit point at a velocity $v = c/3$, unmodified and undistorted, keeping the total charge. The waveshapes of channel-base lightning current can be characterised through different mathematical expressions. Double exponential [73] and Heidler function [74] are mathematical expressions widely used in studying the effects of lightning. Nonetheless, Heidler function provides more realistic results. Thus, this current waveform is pre-defined according to the IEC standard 62305-2 [75], in particular using the expression for a short return flash initiated by an upward leader from exposed structure to cloud. The analytical expression of the channel base current, according to [74,75] is then:

$$i(0,t) = I_{max}\frac{(t/\tau_1)^n}{1+(t/\tau_1)^n} e^{-\frac{t}{\tau_2}} \quad (7)$$

Peak current $I_{max}(20\,\text{kA})$, rise time constant, τ_1 (0.2 μs), delay time constant, τ_2 (100 μs), and the factor about current rise speed, n (10), are four important parameters that indicate lightning current waveshape characteristics. To simulate the lightning current waveform, according to [75,74] the values in brackets are chosen (see Fig. 3).

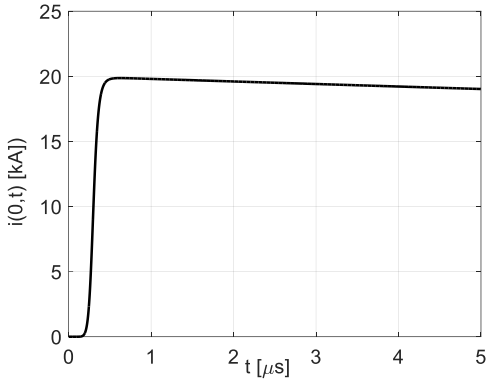

Fig. 3. *Lightning current, according to IEC 62305-2 [76]*

3. Geometrical model of a PV module

3.1. PV cells

A typical PV module (Fig. 4a) has the structure shown in Fig. 4b, realized by interconnecting a number of elementary PV cells. Interconnection between cells is realized by lengthening the main lines of the front metal grid in each cell and linking them to the plated back of the next cell (see Fig. 4c for a detail). This interconnection in series-parallels is equivalent to straight wires which form geometric conductor loops (see equivalent red line Γ in Fig. 4b for a series interconnection) [52]. The resulting path (line Γ) is composed partly by the cell itself, and partly by the metallic connections joining cells. At the ends of the wires, two terminal lines are extracted as the positive and negative electrodes of the PV module.

The aim of the present paper is the analysis and computation of the effect of EM fields radiated by lightning strikes when the PV module is in open circuit condition. For such a reason, the wirings complex 3D shape is modelled by connections having a thin-wire structure and developing on a planar path, since the up-down transitions on different sides of the PV cell do not contribute significantly to the concatenated magnetic flux and, consequently, to induced voltages. For the same reason, only one busbar is considered in the model for each PV cell, while the presence of a higher number of busbars will be considered in a subsequent paper, in which the effects of overcurrent flowing in a connected load will be studied.

In the considered geometry, the internal loop (line Γ) determines the differential-mode area A_{DM} (yellow). Furthermore, the conducting frame around the PV module determines a second closed loop which encloses the frame area A_F (blue). The relative complement of the internal loop (area A_{DM}) and the frame loop (area A_F) determines a third closed loop which is the common-mode area A_{CM} (Fig. 4b).

3.2. Metallic frame

PV modules are usually framed in an aluminium case for structural and safety reasons. While the planar footprint of the frame is a simple rectangle, as already shown in Fig. 4b, its cross section has a complex shape (see Fig. 4d), that must be considered in the modelling of the device. In this work, the cross section equivalent area is used in the equivalent resistance and self inductance computation [77].

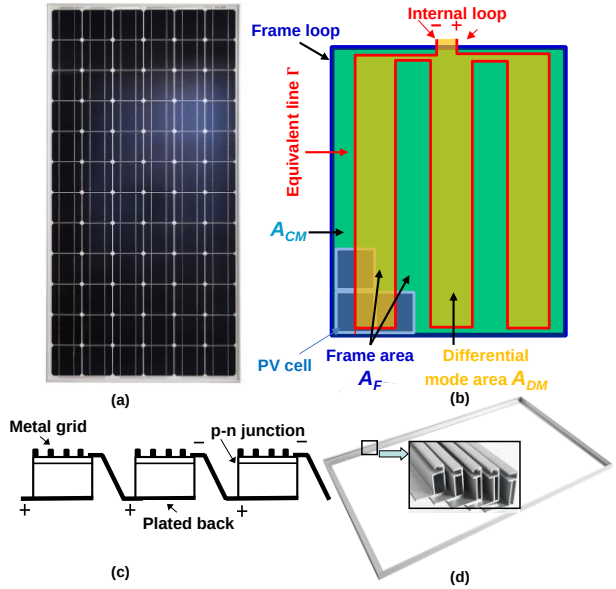

Fig. 4. *PV module: (a) Picture of a representative 270-Wp module, (b) schematic representation of different loops and areas for its geometrical modelling, (c) Schematic electrical connection in a PV cell and between cells, (d) Frame of a representative 270-Wp module*

4. Lightning channel coupling

A straightforward dimensional analysis [61], considering the PV module dimensions (in the order of 1 m x 1 m), its distance from the ground (in the order of 1 m in this analysis), and the amplitude of EM fields at typical distances (the lightning current generates a peak flux density in the order of 4 mT at 5 m, while the amplitude of electric field at ground during thunderstorms is in the order 4 kV/m) and spectral content of EM fields from lightning strikes (maximum frequency content in the range of 5 MHz) [78] shows that the most relevant effect is due to inductive coupling with strike current, generating significant overvoltages both between PV circuit terminals (differential-mode voltage) and between terminals and metal frame (common-mode voltage [2]). This is confirmed by experimental evidence [52]. In this paper, the common- and differential-mode overvoltages are computed using a semi-analytical method, while the effects of such overvoltage on insulating materials is studied by assuming a 3D FEM model of the module and its frame and using values from the semi-analytical model.

The shape of the channel is not influenced by the dynamics of the EM field, and therefore, the inductive effect of the lightning current on the active circuit of a PV module (i.e., induced voltage in differential-mode) can be modelled by computing the lightning flux linked across the area A_{DM}, previously defined in Fig. 4b. Since the conducting frame of the PV module is short-circuited, the lightning flux variation in this frame will cause an additional current (frame current), and consequently a magnetic flux across A_{DM}, that cannot be neglected. Therefore, induced voltage in differential-mode will be modelled by the superposition of lightning and frame current's generated fluxes.

Moreover, as discussed above, the presence of the conducting frame around the PV module originates a second area A_{CM}, laying between the active circuit loop and the PV module frame loop (see Fig. 4b). Similarly to induced differential-mode voltage, the inductive effect of lightning and frame flux between the active circuit of PV cells and the earthed frame is taken into account and induced voltage in common-mode are computed.

Since nearby lightning strikes does not directly hit the PV power system, lightning current does not flow into grounded metallic construction neither into the grounding system and there is no ground voltage rise at the earth termination system. Only the induction coupling due to LEMP has to be considered. Galvanic and resistive coupling [2,19] should not be accounted.

The differential voltage across the PV module terminals is computed by time-derivation of the linked flux, and can be modelled by means of independent voltage sources in the PV module equivalent circuit represented in Fig. 5 where:

(i) R_{FR} is the equivalent resistance of the aluminium frame, computed taking into account the frame shape and dimension; L_{FR} is the self-inductance of the frame, computed using the formula for thin rectangular coils [79] and a correction factor to take into account its cross section (obtained by fitting experimental data in [52]).

(ii) R_s (L_s) is the series resistance (parasitic inductance) of the wiring on the cells and cables of PV module; R_{s_PVM} (R_{p_PVM}) is the series (shunt) resistance of PV cell connections in the AC (frequency) dynamic model of a PV module [80- 86]; similarly C_{p_PVM} is the shunt capacitance of this dynamic model. These latter parameters generally depend on frequency and voltage.

(iii) V_{PVM} and V_{FR} are the voltages generated by lightning current magnetic flux across A_{DM} and A_F, respectively, computed by line integrating the vector potential as per eq. (5) along bounding lines, and finally $M_{FR\text{-}PVM}$ is the mutual inductance between frame and PV internal circuit, computed by line integrating the vector potential generated by a unit current in the frame along the equivalent connections line in the PV module [77].

(iv) $R_{s\text{-}lek\_PVM}$ ($R_{p\text{-}lek\_PVM}$) is the series (parallel) insulation resistance of PV module between active parts and the frame [55] that characterizes capacitive coupling; similarly $C_{p\text{-}leak\_PVM}$ is the shunt capacitance of this model. These parameters depend on frequency, voltage and weather conditions.

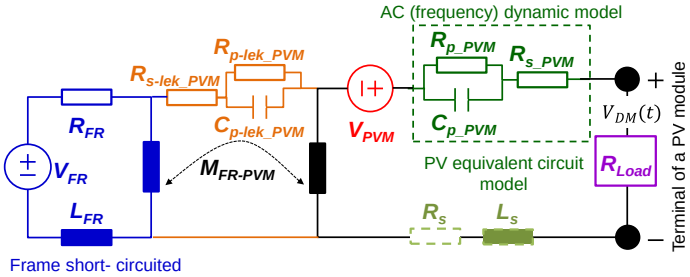

Fig. 5. *AC (frequency) dynamic model of a PV module*

5. Method validation of the codes developed to calculate induced voltages

In order to validate the described model for computation of induced voltages on a PV module, two types of tests have been carried out. In test a) results are compared with a simple FEM model of the lightning channel; in test b)

induced voltages have been compared to experimental tests described by Stern et al. in [52].

5.1. Test a - Comparison with FEM model

In order to validate the computational model, as a first example a straight lightning channel 100 m high on a highly conducting plane, fed by the current waveform reported in Fig. 3 has been considered. The magnetic flux linked by a 0.5 m x 0.5 m vertical square 20 m away from the channel has been computed both by using the proposed approach and by a FEM commercial package [87].

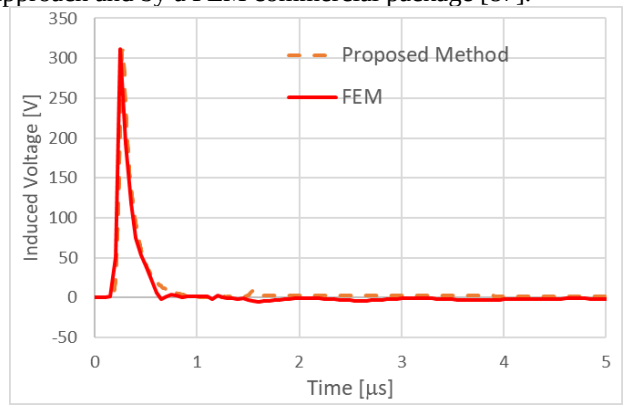

Fig. 6. *Comparison of voltage waveforms induced on a 0.5x0.5 m square plate by a 100 m high straight channel, with the IEC current in Fig. 3. Dotted: results from the proposed method, solid line: results from a 2D axially symmetric FEM computation*

The comparison of voltage waveforms reported in Fig. 6 shows the accuracy of the proposed model.

5.2. Test b - Comparison with experimental results in Stern et al. [52]

As a second validation test, the experimental set-up proposed in [52] was considered, in which a straight metal wire is connected to a capacitor bank and to a resistor, providing a specific current waveform.

We numerically simulated the experiment using a single wire, about 1.6 m long and 0.8, 1.5 and 2 m away from the PV module (Fig. 7), both neglecting and considering the effect of the surrounding frame, as reported in [52].

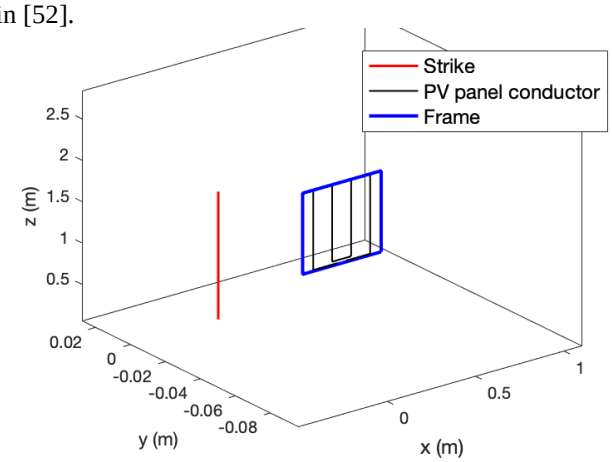

Fig. 7. *Geometry of lighting channel and PV module in the validation vs. [52] experimental data. The red line (Strike) simulates the lightning strike, while the black line (PV module conductor) simulates the PV module connection, as in Fig. 4*

The induced voltages are presented in Fig. 8, in which the strike current waveform is coloured in blue. The comparison with data presented in [52] is summarized in Table 1 and show a satisfactory agreement. The comparison of the measured and calculated results of all these effects demonstrates the validity of the developed model and the performed procedure.

Note that ref [52] does not specify conductor's length, neither details of the frame (material, geometry, and so on) so we have chosen the values providing the best fit at the closest distance. At larger distance between wire and PV module, the connections to the circuit and the actual geometry become relevant for the correct modelling, but those data are not available.

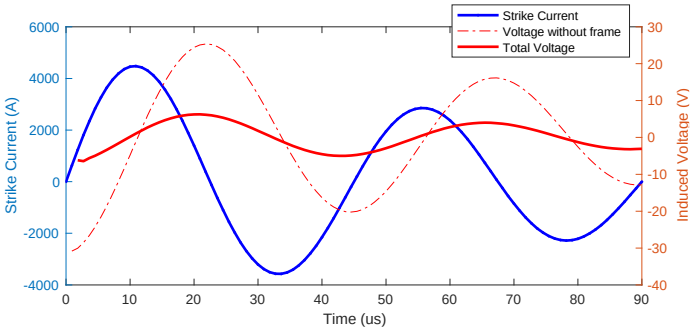

Fig. 8. *Induced voltage and current waveforms in the validation vs. experimental data in [52]*

Table 1. *Comparison of induced voltages in differential-mode for the experiment in Stern et al. [52]*

Distance (m)	Voltage	Measured (V)	Computed (V)	Our model (V)
0.8	No frame	21.3	22.1	21.7
	Frame	4.3	4.3	4.7
1.5	No frame	6.9	9.1	7.8
	Frame	1.5	1.8	1.7
2.0	No frame	3.5	5.8	4.7
	frame	0.8	1.1	1.0

6. Results

6.1. Test system description

In order to assess the capabilities of the proposed approach in the forecast of overvoltage induced on PV modules, we have considered a representative 270-Wp module laying on the ground and tilted by 45° to maximize exposition to solar light. We have run a MonteCarlo analysis by generating a high number of random lighting channels, hitting at different distances from the PV module. The lightning current waveform adopted is shown in Fig. 3.

Table 2, together with Fig. 9, shows the 270-Wp module used in the experiment and its dimensioned drawing. For practical numerical simulations, the parameters for the AC (frequency) dynamic model of a PV module are according to [55,81,82]. The parameter is calculated at a frequency of 1 MHz, which is the dominant oscillating frequency of the measured result.

Only one busbar is considered in the model for each PV cell as shown in Fig. 7. Relevant standard deviations

$(\sigma_{\alpha_1}, \sigma_{\alpha_2}\sigma_{\lambda\min})$ are assumed be 0.05 rad for both angles, and 1/10 of the smallest wavelength in the electromagnetic wave for length.

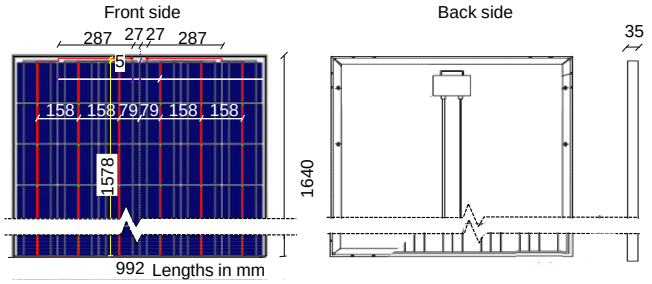

Fig. 9. *Front and back side view of the of the representative 270-Wp module*

Table 2. *Data of the representative 270-Wp module*

Electrical data	Frame				
Number of cells (matrix)	Material	Shape	Thickness (mm)	Section size (mm)	Average area size (mm^2)
6 *x*10 156mm*x*156mm	Anodized aluminium	L-profile	1.5 mm	35 *x* 35	163.65

6.2. Lightning overvoltages

In order to assess the impact of the complex shape of the lightning channel, and taking advantage of the promptness of the proposed method, a statistical analysis has been developed, by considering 100 different LC, and evaluating the voltage induced by the IEC current waveform on a 45° tilted PV, described in Table 2 and Fig. 9. Each channel is 1000 m high. A few examples of adopted channels are reported in Fig. 10; they can be considered as representative of the geometrical structure of the LC.

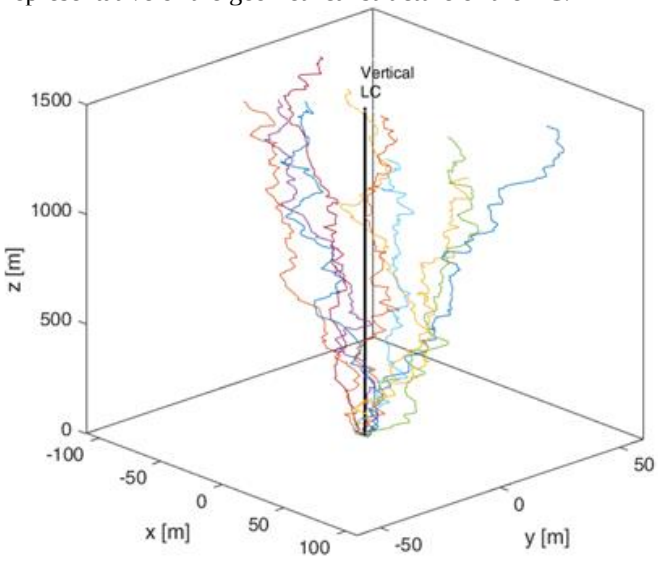

Fig. 10. *Ten examples of LC geometries from 100 Monte Carlo simulation*

Three different distances between LC hitting point on the ground and the PV module were considered, namely 5, 20 and 50 m. Differential-mode induced voltages waveforms $V_{DM}(t)$ for a selection of the 100 channels, corresponding to geometries in Fig. 10, are reported in Fig. 11 for 5 m (-a) 20 m (-b) and 50 m (-c) respectively, not considering the frame effect. The same voltages are reported in Fig. 12 when the presence of the frame is considered, and finally common-mode voltages are reported in Fig. 13. The thicker black curve corresponds in all cases to the voltage induced by a vertical channel.

Average and standard deviations for the 100 cases are reported in Tables 3 to 5, both for the voltage max values and for the "duration" of the event, defined as the time required for the voltage to stably fall below the 5% of the peak value.

When comparing induced voltages in differential and common-mode, results underline that slightly higher values are achieved when the common-mode is taken into account, in spite of, surprisingly, this mode has never been fully considered before now. Extremely interesting is the effect of the presence of the metal frame: it decreases significantly the induced voltages, even about ten times; Consequently, PV modules with a metal frame should be preferred to modules without a metal frame.

Without frame, and under common-mode, voltages up to some kV can be induced in a single PV module. If we consider the SWC of live parts of modules [2,8] it is not difficult to predict that insulation failures in PV modules can be caused by inductive couplings of nearby lightning strikes. Moreover, it is important to note that SWC between active parts of a PV module (that related with differential-mode) is higher than its SWC between active parts and ground [2,13,15].

Regarding the distance between strike hitting point on the ground and the PV module it is shown that it plays an important role. Thus, induced voltage decreases more than twice the distance.

Table 3. *Induced voltages in differential-mode for 100 Monte Carlo simulations -no frame effect*

Distance		5 m	20 m	50 m
Induced voltage (V)	Average	2513	416	125
	Std. dev	1444	101	18
	Vertical strike	*2191*	*406*	*128*
Time to 5% of peak(μs)	Average (ms)	0.58	1.46	2.79
	Std. dev	0.11	0.55	0.35
	Vertical strike	*0.54*	*0.83*	*1.28*

Table 4. *Induced voltages in differential-mode for 100 Monte Carlo simulations -with frame effect-*

Distance		5 m	20 m	50 m
Induced voltage (V)	Average	205	26	8
	Std. dev	231	9	2
	Vertical strike	*134*	*24*	*8*
Time to 5% of peak(μs)	Average (ms)	1.12	2.83	3.14
	Std. dev	0.73	0.34	0.07
	Vertical strike	*0.39*	*0.67*	*1.06*

Table 5. *Induced voltages in common-mode for 100 Monte Carlo simulations*

Distance		5 m	20 m	50 m
Induced voltage (V)	Average	2761	440	131
	Std. dev	1832	116	20
	Vertical strike	*2296*	*426*	*135*
Time to 5% of peak(μs)	Average (ms)	0.61	1.77	2.99
	Std. dev	0.21	0.64	0.23
	Vertical strike	*0.54*	*0.83*	*1.28*

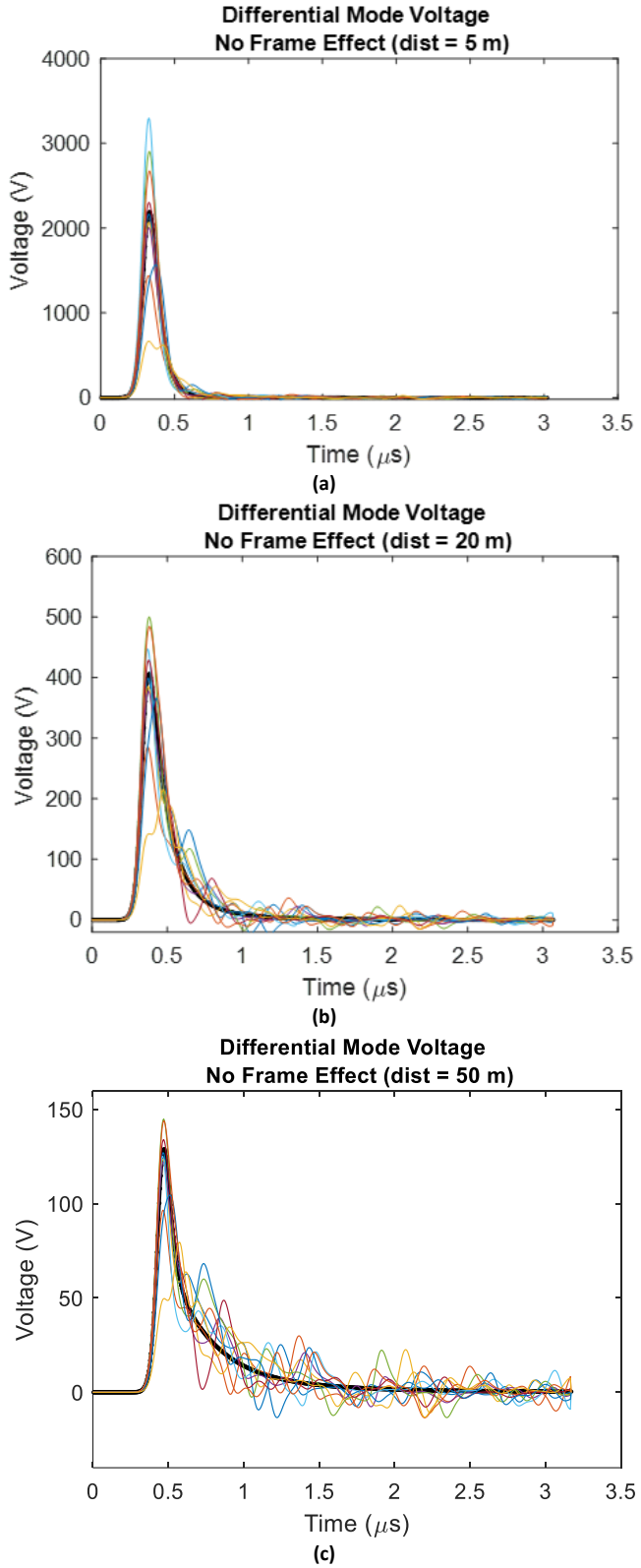

Fig. 11. *Ten examples of induced voltage waveforms in differential-mode selected from 100 Monte Carlo simulations (without frame effect)*

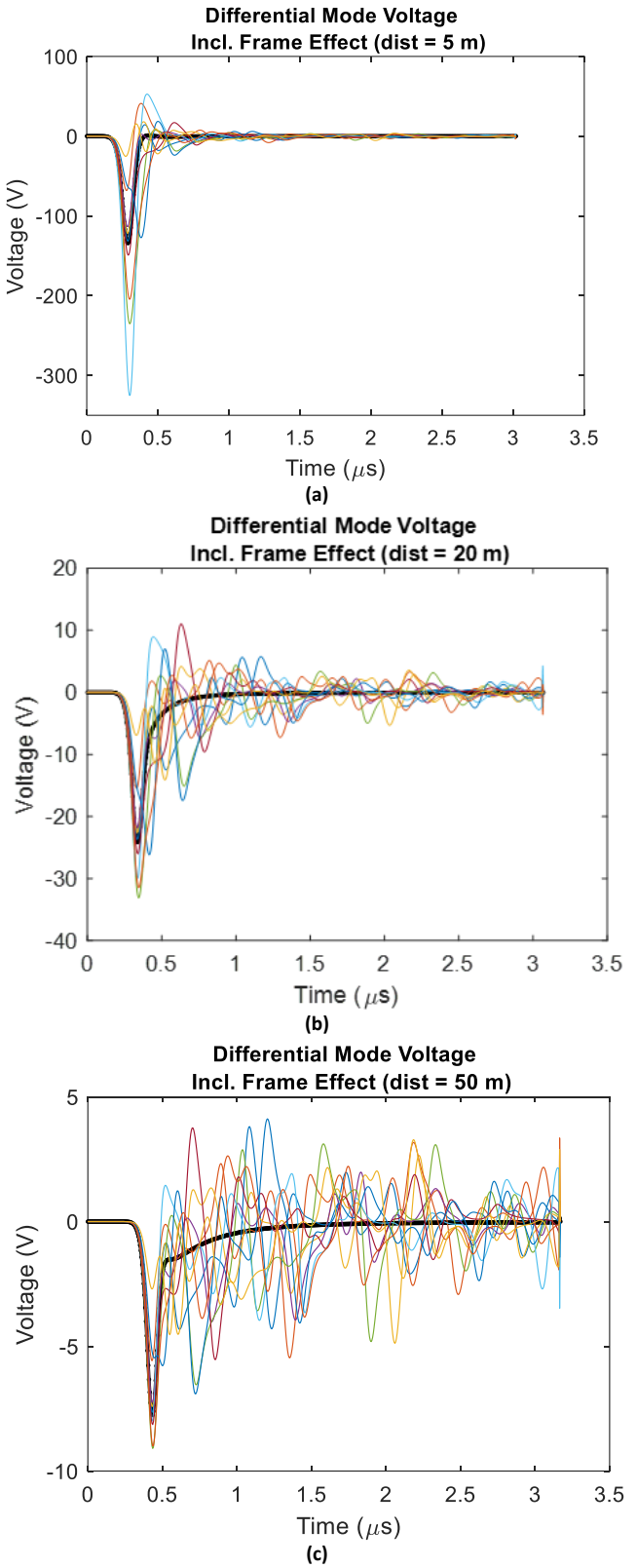

Fig. 12. *Ten examples of induced voltage waveforms in differential-mode selected from 100 Monte Carlo simulations (with frame effect)*

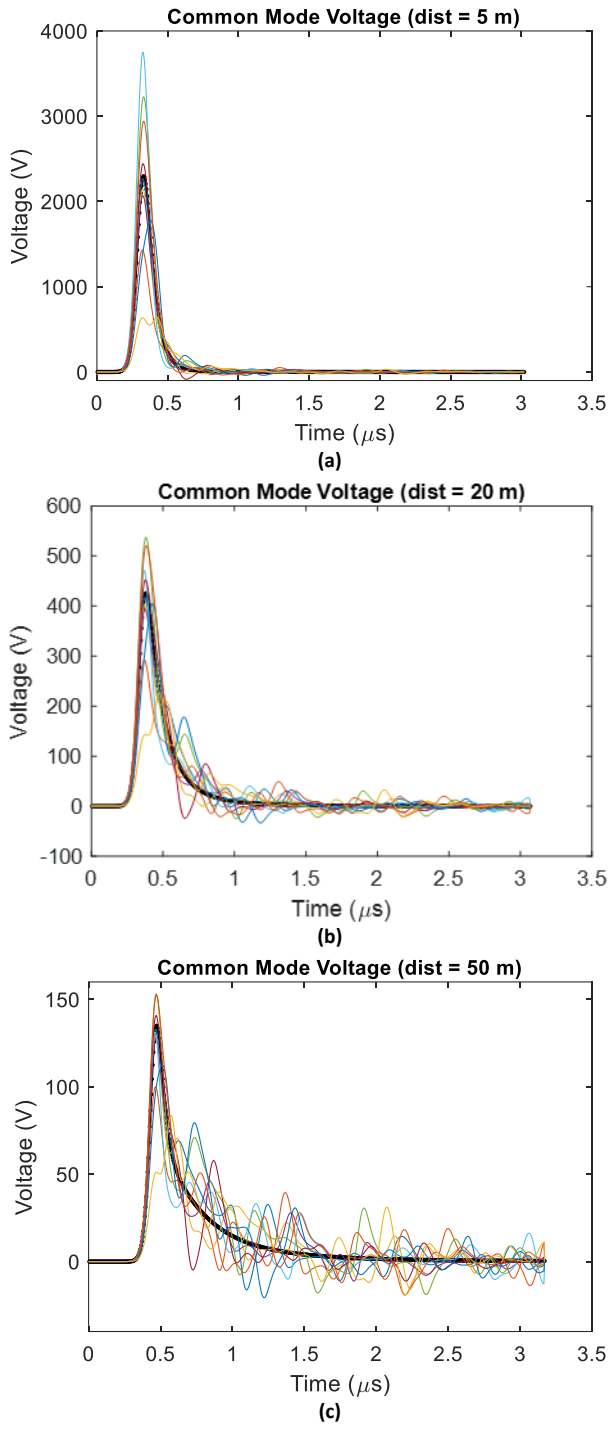

Fig. 13. *Ten examples of induced voltage waveforms in common-mode selected from 100 Monte Carlo simulations*

From the above tables it is also evident that the channel geometry plays a primary role in the assessment of the electromagnetic stress on a PV panel. The closer the LC hits the ground, the more relevant is the effect of tortuosity. As an example we can analyse the results when the frame effect is taken into account. In close proximity of the channel base (i.e. at 5 m), the average peak of differential mode voltage induced by a tortuous LC can be 34% higher than the value produced by a vertical path (Table 4); moreover the average "duration" of the stress can be even 65% longer. Furthermore, it should also be considered that the respective standard deviations are remarkable at close range and, consequently, the maximum stress can be extremely relevant. Similar conclusions can be drawn also neglecting the frame-effect or considering the common common-mode voltages

The deviations from the vertical channel tend to decrease with distance from the point of impact of the lightning channel. In fact, at 50 m away from the panel, the average peak of the induced voltage, in all the cases considered, is practically the same both for a tortuous or a vertical lightning path. Anyway, the value of the standard deviations still suggest that the statistical variability of the channel geometry cannot be neglected when dimensioning the lightning protection system of a PV module and the vertical channel assumption can only be used for a first step estimate.

In this framework, a 3D FEM model can help designers to estimate the distribution of the electrical stress in a PV panel subjected to a close lightning strike. An electro quasistatic model can be adopted since the maximum geometrical distance is much smaller than the minimum wavelength. Fig. 14a shows the time evolution of the electric field amplitude in the middle of the PV panel produced by the common-mode voltage induced by an indirect strike at 20 m. The relative 3D representation of the electric field norm at time instant t=0.5 μs and the isolines of the electric field at the PV panel middle plane are then shown in Fig. 14b and Fig. 14c, respectively.

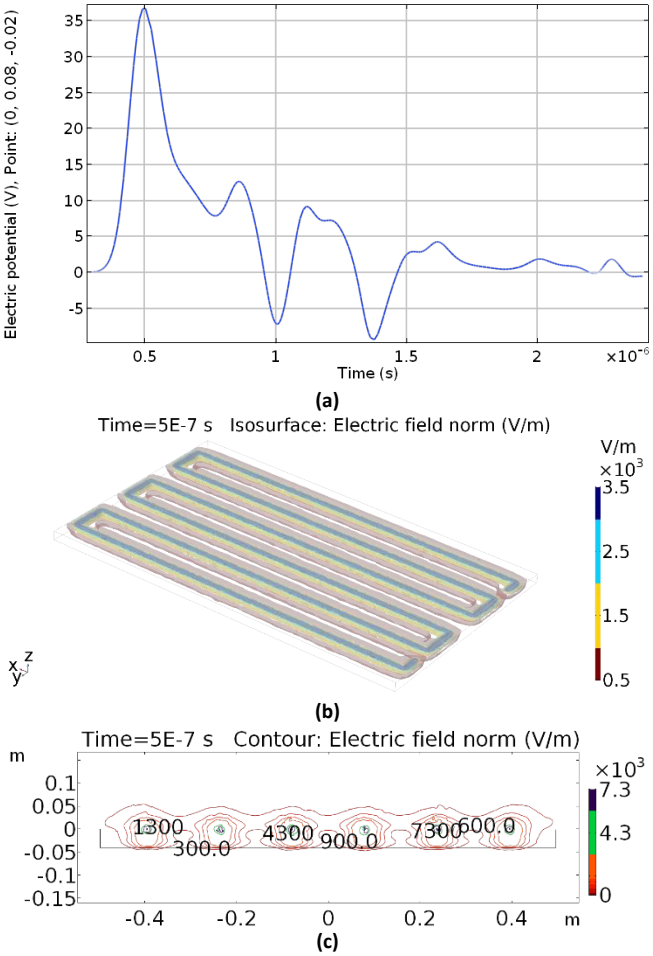

Fig. 14. *Electric field map due to common-mode voltage induced by an indirect strike at 20 m: a) Time evolution of field amplitude in the middle of the PV panel, b) 3D representation of the electric field norm at t=0.5 μs, c) isolines of electric field at the PV panel middleplane*

7. Conclusions

The novelty contribution of our research lies in the application of advanced method to evaluate the electromagnetic field generated by tortuous lightning channels, applied to the assessment of the voltages induced on a PV module by indirect striking. The lightning channel has been modelled as a sequence of randomly generated segments, with random variations of direction between adjacent segments. A semi-analytical method to evaluate electromagnetic fields has been used. The PV module has been modelled in terms of the connecting conductor path among cells, creating a surface for the definition of concatenated flux.

It has been found that the usual approach to model the channel as a vertical line may lead to significant underestimate of the induced voltage, especially for farther striking points, where the whole channel impacts on the voltage. We found that with the increasing strike height the induced voltage also increases except the line to ground voltage.

Results have highlighted that the induced voltage values in common-mode are slightly higher than those for differential-mode, in spite of this mode has not been studied before now, and it is necessary its assessment to design the surge protection in PV systems (selection of SPDs).

Consequently, the method and models presented in this paper may assist engineers to perform the design of the lightning and surge protection in PV systems.

8. References

[1] DEHN., 'Lightning and Surge Protection for Free Field PV Power Plants' (DEHN, 2014), p. 15

[2] Hernandez, J.C., Vidal, P.G., Jurado, F.: 'Lightning and surge protection in photovoltaic installations', IEEE Trans. Power Del., 2008, 23, (4), pp. 1961–1971

[3] Uman, M.A.: 'All about lightning' Toronto: Dover, 1986, pp. 1–158

[4] Ahmada, N.I., Ab-Kadira, M.Z.A., Izadi, M., et al.: 'Lightning protection on photovoltaic systems: A review on current and recommended practices', Renew. Sust. Energ. Rev., 2018, 82, (1), pp. 1611–1619

[5] Häberlin, H.: 'Interference voltages induced by magnetic fields of simulated lightning currents in PV modules and arrays'. Proc. 17th European Photovoltaic Solar Energy Conference, Munich, Germany, 2001, pp. 2343–2346

[6] Becker, H.: 'Lightning and overvoltage protection in photovoltaic and solar thermal systems'. TÜV Rheinland. 2000

[7] Belik, M.: 'PV panels under lightning conditions'. Proc. 15th International Scientific Conference on Electric Power Engineering, Brno, Czech Republic, 2014, pp. 367–370

[8] Jiang, T., Grzybowski, S.: 'Electrical degradation of Photovoltaic modules caused by lightning induced voltage'. Proc. 2014 IEEE Electrical Insulation Conference, Philadelphia, PA, USA, 2014; pp. 107–110

[9] NEDO., 'Analysis and evaluation of lightning damage condition and damage decrease countermeasure technique of lightning damage for PV systems' 2009

[10] CIGRE WG C4.408: 'Lightning protection of low-voltage networks', CIGRE Technical Brochure. 2013

[11] Yang, H., Liu, X.: 'Design of PV charge and discharge controller in insulator monitoring system'. Proc. 2011 2nd International Conference on Artificial Intelligence, Management Science and Electronic Commerce, Dengleng, 2011, pp. 2039–2042

[12] IEC Std. 61000-4-5: 'Electromagnetic compatibility—part 4–5: testing and measurement techniques—surge immunity test', 2014

[13] IEC Std. 60664-1: 'Insulation coordination for equipment within LV systems—part 1: principles, requirements and tests', 2007

[14] IEC Std. 61730-2: 'PV module safety qualification—part 2: requirements for testing', 2016

[15] Funabashi, T.: 'Integration of distributed energy resources in power systems implementation, operation and control' (Toshihisa Funabashi, 2016)

[16] Dechthummarong, C., Thepa, S., Chenvidhya, D., et al.: 'Lightning impulse test of field-aged PV modules and simulation partial discharge within MATLAB'. Proc. 9th International Conference on Electrical Engineering/ Electronics, Computer, Telecommunications and Information Technology, Phetchaburi, 2012, pp. 1–4

[17] Méndez, Y., Acosta, I., Rodriguez, J.C., et al.: 'Effects of the PV-generator's terminals connection to ground on electromagnetic transients caused by lightning in utility scale PV-plants'. Proc. 33rd International Conference on Lightning Protection, Estoril, 2016, pp. 1–8

[18] Kern, A., Krichel, F.: 'Considerations about the lightning protection system of mains independent renewable energy hybrid-systems. Practical experiences', J. Electrostatics, 2004, 60, pp. 257–263

[19] Sekioka, S.: 'Lightning protections of renewable energy generation systems' In integration of distributed energy resources in power systems. (Academic Press, 2016), 2016, pp. 193–228

[20] Zaini, N.H., Kadir, M.Z.A.Ab., Radzi, M.A.M., et al.: 'Lightning surge analysis on a large scale grid-connected solar photovoltaic system', Energies, 2017, 10, (12), pp. 2149–

[21] Ahmad, N.I., Ab-Kadir, M.Z.A., Izadi, M., et al.: 'Lightning protection on photovoltaic systems: A review on current and recommended practices', Renew. Sust. Energ. Rev., 2018, 82, (1), pp. 1611–1619

[22] Davidson, D.B.: 'A review of important recent developments in full-wave CEM for RF and microwave engineering'. Proc. 2004 3rd International Conference on Computational Electromagnetics and Its Applications, Beijing, 2004, pp. PS/1–PS/4

[23] Oufi, E., Alfuhaid, A., Saied, M.: 'Transient analysis of lossless singlephase nonuniform transmission lines', IEEE Trans. Power Del., 1994, 9, (3), pp. 1694–1700

[24] Zou, J., Lee, J., Ji, Y., et al.: 'Transient simulation model for a lightning protection system using the approach of a coupled transmission line network', IEEE Trans. Electromagn. Compat., 2007, 49, (3), pp. 614–622

[25] Townbridge, C.W., Sykulski, J.K.: 'Some key developments in computational electromagnetics and their attribution', IEEE Antennas Propag. Mag., 2006, 42, (6), pp. 503 – 508
[26] Harrington, R.F.: 'Field computation by moment methods', (Macmillan, New York, 1968)
[27] Wang, S., He, J., Zhang, B., et al.: 'A time-domain multiport model of thin-wire system for lightning transient simulation', IEEE Trans. Electromagn. Compat. 2010, 52, pp. 128–135
[28] Wang, S., He, J., Zhang, B., et al.: 'Time-domain simulation of small thin-wire structures above and buried in lossy ground using generalized modified mesh current method', IEEE Trans. Power Deliv. 2011, 26, pp. 369–377
[29] Jin, J.M.: 'The finite element method in electromagnetics', (John Willey & Sons, Inc., 2nd edn. New York, 2002)
[30] Volakis, J.L., Chatterjee, A., Kempel, L.C.: 'Finite element method for electromagnetics', (IEEE Press, Oxford University Press, 1997)
[31] Yee, K.S.: 'Numerical solution of initial boundary value problems involving Maxwell's equations in isotropic media', IEEE Antennas Propag. Mag., 1966, 14, pp. 302-307
[32] Sullivan, D.M.: 'Electromagnetic simulation using the FDTD method', (Wiley – IEEE Press., 2000)
[33] Poljak, D., Brebbia, C.A.: 'Boundary Element Methods for Electrical Engineers', WIT Press, Boston, 2005
[34] Ishii, M., Baba, Y.: 'Numerical electromagnetic field analysis of tower surge response', IEEE Trans. Power Deliv., 1997, 12, (1), pp. 483–488
[35] Wang, S., He, J., Zhang, B.: 'A Time-domain multiport model of thin-wire system for lightning transient simulation', IEEE Trans. Electromag. Compat., 2010, 52, (1). Pp. 128–135
[36] Baba, Y., Rakov, V.A.: 'Voltages induced on an overhead wire by lightning strikes to a nearby tall grounded object', IEEE Trans. Electromag. Compat., 2006, 48, (1), pp. 212–224
[37] Noda, T., Yokoyama, S.: 'Development of Surge Simulation Code Based on Finite-Difference Time-Domain Approximation of Maxwell's Equations'. Proc. 2014 International Power Electronics Conference, Hiroshima, 2014, pp. 1-5
[38] Noda, T., Tatematsu, A., Yokoyama, S.: 'Improvements of an FDTD based surge simulation code and its application to the lightning overvoltage calculation of a transmission tower', Electr. Power Syst. Res., 2007, 77, (11), pp. 1495–1500
[39] Rubinstein, M., Uman, M.A.: 'Methods for calculating the electromagnetic fields from a known source distribution: application to lightning', IEEE Trans. Electromag. Compat., 1989, 31, (2), pp. 183–189
[40] Tu, Y., Zhang, C., Hub, J., et al.: 'Research on lightning overvoltages of solar arrays in a rooftop photovoltaic power system', Electr. Power Syst. Res., 2013, 94, pp. 10–15
[41] Charalambous, C.A., Kokkinos, N.D., Christofides, N.: 'External lightning protection and grounding in large-scale photovoltaic applications', IEEE Trans. Electromag. Compat., 2014, 56, (2), pp.427–434
[42] Yamamoto, K., Takami, J., Okabe, N.: 'Overvoltage on DC side of power conditioning system caused by lightning stroke to structure anchoring photovoltaic panels', IEEJ Trans. Power Energy, 2012, 132-B, (11), pp. 903–913
[43] Hossain, A., Ahmed, R.: 'Analysis of indirect lightning phenomena on solar power system', J. Electrical Engineering, 2014, 21, (4), pp. 127–133
[44] Benesova, Z., Haller, R., Birkl J., et al.: 'Overvoltages in photovoltaic systems induced by lightning strikes'. Proc. 2012 International Conference on Lightning Protection, Vienna, 2012, pp. 1-6
[45] Fuangfung, Y., Sinthusonthishat S., Yutthagowith, P.: 'A software tool for induced voltages and currents calculation caused by lightning electromagnetic field in PV systems'. Proc. 2015 12th International Conference on Electrical Engineering/Electronics, Computer, Telecommunications and Information Technology, Hua Hin, 2015, pp. 1–4
[46] IEC 62305-4: 'Protection against lightning - part 4: electrical and electronic systems within structures', 2010
[47] Takada, T., Ishii, M.: 'Lightning-induced voltages around PV panel on ground'. Proc. IEEJ Technical Meeting on HV Engineering, HV-11-90, 2011–12 (In Japanese)
[48] Azhari, M.E.: 'Lightning-induced voltage on DC power line of PV panel'. Masters dissertation, The University of Tokyo, 2013
[49] Kokkinos, N., Christofide, N., Charalambous, C.: 'Lightning protection practice for large-extended photovoltaic installations'. Proc. 2012 International Conference on Lightning Protection, Vienna, 2012, pp. 1–5
[50] Sakai, K., Yamamoto, K.: 'Lightning protection of photovoltaic power generation system: Influence of grounding systems on overvoltages appearing on DC wirings'. Proc. 2013 International Symposium on Lightning Protection, Belo Horizonte, 2013, pp. 335–339
[51] Hernandez, Y.M., Ioannidis, D, Ferlas, G, et al.: 'An experimental approach of the transient effects of lightning currents on the overvoltage protection system in MW-class photovoltaic plants. Lightning Protection'. Proc. 2014 International Conference on Lightning Protection, Shanghai, 2014, pp. 1972–1977
[52] Stern, H., Karner, H.C.: 'Lightning induced EMC phenomena in photovoltaic modules'. Proc. 1993 International Symposium on Electromagnetic Compatibility, Dallas, TX, USA, 1993, pp. 442-446
[53] Zhang, C., Tu, Y., Hu, J., et al.: 'Study of induced overvoltage on solar arrays in Lightning'. Proc. 2011 7th Asia-Pacific International Conference on Lightning, Chengdu, 2011, pp. 852-857
[54] Petrarca, C., Minucci, A., Andreotti, A.: 'On the influence of channel tortuosity on electric fields generated by lightning return strokes at close distance', Prog. Electromagn. Res. B, 2017, 74, pp. 61–75

[55] Hernández, J.C., Vidal, P.G., Medina, A.: 'Characterization of the insulation and leakage currents of PV generators: Relevance for human safety', Renew. Energ., 2010, 35, (3), pp. 593–601.
[56] Dechthummarong, C., Chenvidhya, D., Jivacate, C., et al.: 'Experiment and simulation impulse partial discharge behavior in dielectric encapsulations of field-aged PV modules', Proc. 2011 37th IEEE Photovoltaic Specialists Conference, Seattle, WA, 2011, pp. 3109–3112
[57] Sekioka, S.: 'An experimental study of sparkover between a rod and a photovoltaic panel', Proc. 2012 International Conference on Lightning Protection, Vienna, Austria, 2012, pp. 1–5
[58] IEC Std. 62305-1: 'Protection against lightning—part 1: general principles', 2006
[59] Watt, A.D.: 'ELF electric fields from thunderstorms', J. Research National Bureau Standards-D, 1960, 64D, (5), pp. 425–433
[60] Haus, H.A., Melcher, J.R.: 'Electromagnetic Fields and Energy', Prentice Hall, 1988
[61] Sakakibara, A.: 'Calculation of induced voltages on overhead lines caused by inclined lightning studies', IEEE Trans. Power Deliv., 1989, 4, pp. 683–693
[62] Andreotti, A., Petrarca, C., Rakov, V.A., et al.: 'Calculation of voltages induced on overhead conductors by nonvertical lightning channels', IEEE Trans. Electromag. Compat., 2012, 54, (4), 860–870
[63] Andreotti, A., De Martinis, U., Petrarca, C., Rakov, V.A., Verolino, L.: 'Lightning electromagnetic fields and induced voltages: Influence of channel tortuosity', General Assembly and Scientific Sympos. 2011 XXXth URSI, Istanbul, Turkey, 2011, art. no. 6050702.
[64] Andreotti, A., Petrarca, C., Pierno, A.: 'On the effects of channel tortuosity in lightning-induced voltages assessment', IEEE Trans. Electromag. Compat., 2015, 57, pp. 1096–1102
[65] Meredith, S., Earles, S., Kostanic, I.: 'How lightning tortuosity affects the electromagnetic fields by augmenting their effective distance', Prog. Electromagn. Res., 2010, 25, pp. 155–169
[66 Petrarca, C.: 'Geometrical and physical parameters affecting distant electric fields radiated by lightning return strokes', Prog. Electromagn. Res. B, 2014, 58, pp. 167–180
[67] Hill, R.D.: 'Analysis of irregular paths of lighting channels', J. Geophys. Res.-Atmos., 1968, 73, (6), pp. 1922–1929
[68] Lupo, G., Petrarca, C., Tucci, V. et al.: 'EM fields generated by lightning channels with arbitrary location and slope', IEEE Trans. Electromag. Compat., 2000, 42, pp. 39–53
[69] Stratton, J.A.: 'Electromagnetic theory', (McGraw-Hill, New York,1941)
[70] Uman, M.A.: 'Lightning return stroke electric and magnetic fields', J. Geophys. Res., 1985, 90, (D4), pp. 6121–6130
[71] Ogata, K.: 'Modern Control Engineering', Prentice Hall, New York, 1976
[72] Uman, M.A., Rakov V.A.: 'Lightning physics and effects', (Cambridge University Press, 2007)
[73] Wang, J., Zhang, X.: 'Double-exponential expression of lightning current waveforms', Proc. 2006 4th Asia-Pacific Conference on Environmental Electromagnetics, Dalian, 2006, pp. 320–323.
[74] Heidler, F., Cvetic, J., Stanic, B.: 'Calculation of lightning current parameters', IEEE Trans. Power Deliv. 1999, 14, pp. 399–404.
[75] IEC Std. 62305-2: ' Protection against lightning - part 2: risk management, 2016
[76] IEC Std. 62305-2: ' Protection against lightning - part 2: risk management, 2016
[77] Chiariello, A. G., Formisano, A., Martone, R.: 'A high-performance computing procedure for the evaluation of 3D coils inductance', COMPEL, Vol. 34, No.1, pp-248-260, 2014
[78] Watt, A.D.: 'ELF electric fields from thunderstorms', Journal of Research of the National Bureau of Standards-D. Radio Propagation, 1960, 64D, (5)
[79] Grover, F.W.: 'Inductance Calculations', Dover Publications, New York, 1946
[80] Wade, C.I., Torihara, R., Sakoda, T., et al.: 'Numerical analysis of electrical characteristics of a PV module irradiated by an impulse light flash', J. Int. Counc. Electric. Eng., 2018, 8, (1), pp. 8–13
[81] Application Note B1500A-14, 'IV and CV characterizations of solar/photovoltaic cells using the B1500A' (Agilent Technologies, 2018), pp. 1-5
[82] Poon, J., Jain, P., Spanos, C., et al.: 'Photovoltaic condition monitoring using real-time adaptive parameter identification', Proc. 2017 IEEE Energy Conversion Congress and Exposition, Cincinnati, OH, 2017, pp. 1119–1124.
[83] Cotfas, D.T., Cotfas, P.A., Kaplanis, S.: 'Methods and techniques to determine the dynamic parameters of solar cells: Review', Renew. Sust. Energ. Rev., 2016, 61, pp. 213-221
[84] Kim, K.A., Seo, G., Cho B., et al.: 'Photovoltaic hot-spot detection for solar panel substrings using AC parameter characterization', IEEE Trans. Power Electron., 2016, 31, (2), pp. 1121–1130
[85] Pongklang, T., Chenvidhya, D., Kirtikara, K. et al: 'Voltage and frequency dependent impedances of dye-sensitized solar cell', Energy Procedia, 2014, 52, pp. 536–540
[86] Chenvidhy, D., Kirtikar, K., Jivacate, C.: 'PV module dynamic impedance and its voltage and frequency dependencies', Sol. Energy Mater Sol. Cells, 2005, 86, (2), pp. 243–251
[87] 'COMSOL Multiphysics® v. 5.2.', http://www.comsol.com, accessed 1 October 2018